Princeton Plasma Physics Laboratory

PPPL- 4583

PPPL- 4583

Modification of Particle Distributions By MHD Instabilities I

R. B. White

January, 2011

Prepared for the U.S. Department of Energy under Contract DE-AC02-09CH11466.

Princeton Plasma Physics Laboratory
Report Disclaimers

Full Legal Disclaimer

Trademark Disclaimer

PPPL Report Availability

Princeton Plasma Physics Laboratory:

http://www.pppl.gov/techreports.cfm

Office of Scientific and Technical Information (OSTI):

http://www.osti.gov/bridge

Related Links:

U.S. Department of Energy

Office of Scientific and Technical Information

Fusion Links

Modification of particle distributions by MHD instabilities I

R. B. White[1]

[1]*Plasma Physics Laboratory, Princeton University,*

P.O.Box 451, Princeton, New Jersey 08543

(Dated: December 15, 2010)

Abstract

The modification of particle distributions by low amplitude magnetohydrodynamic modes is an important topic for magnetically confined plasmas. Low amplitude modes are known to be capable of producing significant modification of injected neutral beam profiles, and the same can be expected in burning plasmas for the alpha particle distributions. Flattening of a distribution due to phase mixing in an island or due to portions of phase space becoming stochastic is a process extremely rapid on the time scale of an experiment but still very long compared to the time scale of guiding center simulations. Thus it is very valuable to be able to locate significant resonances and to predict the final particle distribution produced by a given spectrum of magnetohydrodynamic modes. In this paper we introduce a new method of determining domains of phase space in which good surfaces do not exist and use this method for quickly determining the final state of the particle distribution without carrying out the full time evolution leading to it.

PACS numbers: 52.25.Fi, 52.25.Gj

I. INTRODUCTION

The resonant interaction of magnetohydrodynamic (MHD) modes and particle distributions can produce significant modification of the distribution and even induce large scale particle loss through profile avalanche, and is an important topic for magnetically confined plasmas. Low amplitude modes are known to be capable of producing significant modification of injected neutral beam profiles [1–5], and the same can be expected in burning plasmas for the alpha particle distributions. Since magnetic field ripple is a strong function of position, increasing rapidly near the plasma edge, a broadened profile can lead to an increase of stochastic trapped particle ripple loss. Portions of phase space becoming stochastic lead to modification of the particle distribution, a process extremely rapid on the time scale of an experiment but still very long compared to the time scale of guiding center simulations, typically hundreds of hours of computing time to find saturated profiles under the action of a particular mode spectrum. Previous work has focused on quasilinear models for the induced particle transport[6, 7]. The subject of this paper is a method for determining the location and extent of mode-particle resonances and the final state of the particle distribution without carrying out the full time evolution leading to it. In section II we discuss methods of determining the location and breadth of resonances, and introduce a new technique for determining the existence of good Kolmogorov Arnold Moser[8] (KAM) surfaces. In section III we discuss transport induced by the presence of multiple incommensurate modes. In section IV we illustrate the determination of resonant domains with the new technique using some examples employing equilibria and mode spectra observed on DIII-D[2, 3]. In section V we examine a case of overlapping resonances producing a distribution avalanche, and in section VI we construct a process of stochastic annealing, leading to the final state on a time scale large compared to the stochastic diffusion rate. In section VII are the conclusions.

II. RESONANCE DETERMINATION

Using the guiding center drift approximation a particle orbit in an axisymmetric system is completely described by the values of the toroidal canonical momentum P_ζ, the energy E and the magnetic moment μ. Particle spatial coordinates are given by ψ_p, θ, ζ, respectively the poloidal flux coordinate, and the poloidal and toroidal angles. The magnetic field is

given by

$$\vec{B} = g\nabla\zeta + I\nabla\theta + \delta\nabla\psi_p, \tag{1}$$

and in an axisymmetric equilibrium using Boozer coordinates g and I are functions of ψ_p only. The trajectory of the particle motion in the poloidal plane and the toroidal precession of the orbit are independent of the function δ[9, 10].

The guiding center Hamiltonian is

$$H = \rho_\parallel^2 B^2/2 + \mu B + \Phi, \tag{2}$$

where $\rho_\parallel = v_\parallel/B$ is the normalized parallel velocity, μ is the magnetic moment, and Φ the electric potential. The field magnitude B and the potential may be functions of ψ_p, θ and also ζ if axisymmetry is broken. Canonical momenta are

$$P_\zeta = g\rho_\parallel - \psi_p, \qquad P_\theta = \psi + \rho_\parallel I, \tag{3}$$

where ψ is the toroidal flux, with $d\psi/d\psi_p = q(\psi_p)$, the field line helicity. Since we are interested in particle distributions, density is a relevant quantity. Volume is given by $dV = 2\pi J d\theta d\psi_p$, with the Jacobian $J = (gq + I)/B^2$ in Boozer coordinates.

The equations of motion in Hamiltonian form are

$$\begin{aligned} \dot{\theta} &= \frac{\partial H}{\partial P_\theta} \qquad & \dot{P}_\theta &= -\frac{\partial H}{\partial \theta} \\ \dot{\zeta} &= \frac{\partial H}{\partial P_\zeta} \qquad & \dot{P}_\zeta &= -\frac{\partial H}{\partial \zeta}. \end{aligned} \tag{4}$$

Equations for advancing particle positions in time, also in the presence of flute-like perturbations of the form $\delta\vec{B} = \nabla \times \alpha\vec{B}$ with $\vec{B}$ the equilibrium field and $\alpha = \sum_{m,n} \alpha_{m,n}(\psi_p) sin(n\zeta - m\theta - \omega_n t)$ can easily be derived[10]. Including such a perturbation the Hamiltonian for guiding center motion becomes $H = (\rho_c - \alpha)^2 B^2/2 + \mu B + \Phi$, with $\rho_c = \rho_\parallel + \alpha$, and variables ζ, θ, ρ_c, ψ_p. In addition, for ideal MHD perturbations the rapid mobility of the electrons makes the electric field experienced by the ions parallel to the magnetic field equal to zero. In this case it is necessary to add an electric potential Φ to cancel the parallel electric field induced by $d\vec{B}/dt$, with

$$\sum_{m,n} \omega B \alpha_{m,n} e^{i(n\zeta - m\theta - \omega t)} - \vec{B} \cdot \nabla\Phi/B = 0, \tag{5}$$

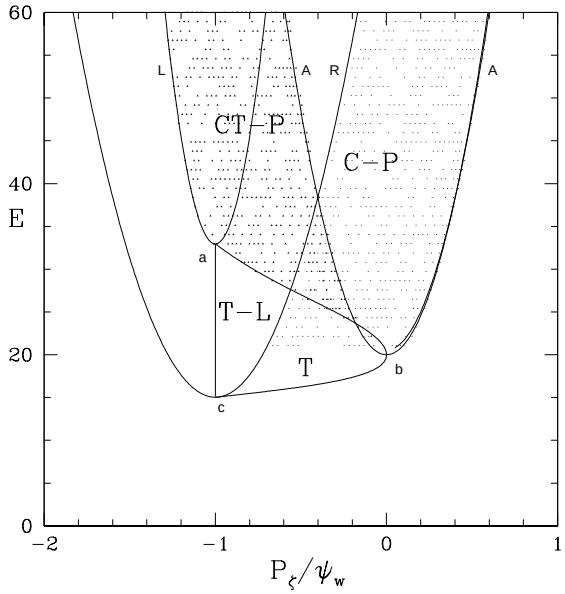

FIG. 1: Plane of P_ζ, E for a range of 20 to 60 keV with $\mu B_0 = 20$ keV, showing domains of confined particles. Shown are co-passing (C-P), counter passing (CT-P), trapped (T) and trapped loss (T-L) domains. The apexes of the parabolas are at $E = \mu B_{max}$ (a), $E = \mu B_0$ (b), $E = \mu B_{min}$ (c).

where we have neglected terms of order α^2. In Boozer coordinates, used in our simulations, taking $\Phi = \sum_{m,n} \Phi_{m,n} e^{i(n\zeta - m\theta - \omega t)}$ the solution is

$$(gq + I)\omega\alpha_{m,n} = (nq - m)\Phi_{m,n}, \tag{6}$$

but in general coordinates where $I = I(\psi, \theta)$ the solution is complicated by the coupling of different poloidal harmonics. The guiding center equations including MHD perturbations are realized using a fourth order Runge-Kutta method in the code ORBIT[11]. The units are conveniently defined by the on-axis gyro frequency ω_0 (time) and the major radius R (distance).

The magnetic moment μ is conserved by the interaction of a particle with a mode with frequency much smaller than the cyclotron frequency, so only P_ζ and E are modified by interaction with it. For a given equilibrium and a fixed value of μ the domains of confined particles in the P_ζ, E plane are given by parabolas defining orbits that make contact with the magnetic axis, the low field side outer boundary, and the high field side outer boundary as well as the trapped-passing boundary.

An example is shown in Fig. 1 for a reversed shear equilibrium with $q = 4.7$ on axis and $q = 9$ at the plasma boundary. Shape and size of the various domains changes with the equilibrium parameters, but the general topology is always similar to that shown. The plane of P_ζ, E is shown for $\mu B_0 = 20keV$ with B_0 the magnetic field on axis and the particle distribution is limited have energy between 20 and 60 keV. The apex of the parabolas are at $E = \mu B_{max}$ (label a) for the high field side (left edge, parabola with label L), $E = \mu B_0$ (label b) for the magnetic axis (parabola with label A), and $E = \mu B_{min}$ (label c) for the low field side (right edge, parabola with label R). The confined counter passing and co-passing orbits share a common triangular region, in which they have the same values of P_ζ and E but opposite signs of pitch. The small eye shaped region near point b consists of potato orbits, particles for which $v_\parallel$ vanishes along the orbit, but which circle the magnetic axis due to drift. The trapped particle domain borders both the co-passing and the counter passing domains at low energy.

To produce a particle distribution of all confined particles with a fixed value of μ, simply launch particles along the entire outboard minor radius ($0 < \psi_p < \psi_w$) (normally $\theta = 0$) with a full range of energy and positive pitch $\lambda = v_\parallel / v$ with $v_\parallel = \sqrt{2E - 2\mu B(\psi_p, \theta)}$ giving all confined co-moving orbits and all confined trapped orbits, thus bounded in P_ζ on the left by the right wall and on the right by the magnetic axis and the lower boundary of the trapped particle domain. Energy is of course limited to $E > \mu B_{min}$. Similarly launch particles along the inboard minor radius (normally $\theta = \pi$) with a full range of energy and negative pitch to produce all confined counter-moving orbits, thus bounded in P_ζ on the left by the left wall and on the right by the magnetic axis. The full distribution of confined orbits with $\mu B_0 = 20keV$ and E between 20 and 60 keV is shown shaded in Fig. 1. This deposition process assumes that the minimum and maximum values of B lie along the midplane. For some highly shaped equilibria this may not be the case and a more complicated procedure must be used. But for most practical applications the particle distribution is given by a neutral beam injection algorithm or an alpha particle birth profile algorithm.

We are interested in the case of the interaction of particles of arbitrary pitch with modes of nonzero frequency. It is fairly easy to assess the effect of a particular mode on a particle distribution by examining a Poincaré plot for a particular choice of either co-moving and trapped or counter-moving particles, which we refer to as a kinetic Poincaré plot to distinguish it from a plot of the magnetic field. Points are plotted in the poloidal cross section

whenever $n\zeta - \omega_n t = 2\pi k$ with k integer, where ζ is the toroidal particle coordinate, and ω_n is the mode frequency. The toroidal motion then gives successive Poincaré points in the poloidal cross section ψ_p, θ, or better, since P_ζ is constant in the absence of perturbations, the P_ζ, θ plane. Individual modes produce islands in the phase space of the particle orbits, which through phase mixing produce local flattening of the particle distribution. In addition, overlap of these islands, the Chirikov criterion, leads to stochastic transport of particles[12, 13]. Such a plot shows the canonical division of orbits into those following good KAM surfaces, isolated islands bounded by separatrices, and stochastic domains. In an ideal situation with a single perturbation the separatrix is a well defined boundary, but in an actual equilibrium it is broadened into a stochastic layer by toroidal coupling or nonlinear coupling to other perturbations.

Energy is not conserved since the mode is time dependent, and for a mode of a single n value the perturbation of the Hamiltonian includes ζ and t only in the form $H(n\zeta - \omega_n t)$. Similarly, canonical toroidal momentum is not conserved. From Hamilton's equations $dP_\zeta/dt = -\partial_\zeta H$, and $dE/dt = \partial_t H$ and thus for fixed n we find that $\omega_n P_\zeta - nE$ is constant in time. To obtain a kinetic Poincaré plot the distribution must be initiated with a fixed value of μ and $\omega_n P_\zeta - nE = c$. A plot with particles of fixed μ and energy E does not give a coherent plot: it contains intersecting surfaces, since it is really an overlaying of plots with different values of c. Choosing the energy to be E_0 at the magnetic axis where $\psi_p = 0$ the pitch on axis is $\lambda_0 = \sqrt{1 - \mu B_0/E_0}$, and $c = g(0)\omega_n \lambda_0 v_0/B_0 - nE_0$. Then for any surface the pitch is $\lambda = \pm\sqrt{1 - \mu B(\psi_p, \theta)/E}$ and finally the velocity on surface ψ_p is the solution to

$$c + \omega_n \psi_p - \frac{g(\psi_p)\omega_n \lambda(v) v}{B} + \frac{nv^2}{2} = 0, \tag{7}$$

which can be solved by Newton's method.

Some progress can be made analytically to determine the location of resonances. A Poincaré point occurs when $n\zeta - \omega_n t = 2\pi k$. For there to be a periodic fixed point in θ with period m' we also require $\Delta\theta = 2\pi l/m'$ between successive points with l integer. Here m' is the number of islands in a poloidal cross section Poincaré plot. The helicity of the resonance is then

$$R(P_\zeta, E, \mu) = \frac{\Delta\zeta - \omega_n \Delta t/n}{\Delta\theta} = \frac{m'}{nl}, \tag{8}$$

which must be rational. Note that the poloidal mode number m does not appear in this expression. For a resonance to appear there must exist integers m', l such that this relation can be satisfied, but this is not a sufficient condition for the formation of an island.

The modification of these quantities due to the perturbation α can be neglected. Converting integrals over time to integrals over θ, we have

$$\Delta\zeta = \int \frac{\dot{\zeta}}{\dot{\theta}} d\theta, \qquad \Delta t = \int \frac{1}{\dot{\theta}} d\theta \tag{9}$$

where the integrands must be evaluated following a closed particle orbit, and for passing particles $\Delta\theta = 2\pi$, but for trapped particles the integrals must be between the bounce points.

To do these integrals one needs ψ_p as a function of θ over the orbit, which can be obtained by equating the two expressions for $\rho_\parallel$,

$$\rho_\parallel = \pm\frac{\sqrt{2E - 2\mu B}}{B} = \frac{P_\zeta + \psi_p}{g}. \tag{10}$$

Given P_ζ, E, μ, θ one thus finds ψ_p and then $\dot{\zeta}$, $\dot{\theta}$, and can perform the integrals[10]. For fixed values of E, μ we scan the range of P_ζ and carry out the integrals, looking for values of P_ζ for which $R(P_\zeta, E, \mu)$ is a low order rational. This determination of the existence of fixed points is not sufficient for the formation of an island, since it is also necessary that the perturbation, of the form $\alpha = \sum_{m,n} \alpha_{m,n}(\psi_p) sin(n\zeta - m\theta - \omega_n t)$ be nonzero at this value of P_ζ, E, μ and also that it be in resonance with the fixed point period, either directly or through toroidal coupling, which normally means that m' is not far removed from m. In performing the scan over P_ζ for rational values of R the relation $\omega_n P_\zeta - nE = c$ is maintained so that the resonance points can be compared to resonances seen in a kinetic Poincaré plot.

Although a Poincaré plot is instructive, it is too time consuming to examine effects on a whole distribution because it gives information on only one line in the P_ζ, E, μ volume and there is no obvious way to automate it. In this paper we introduce a general method for numerically determining the existence of or the destruction of good KAM surfaces.

Consider following two orbits located very nearby one another. Examine a Poincaré section in P_ζ, θ and define the angle χ to give the orientation of the vector joining them in this plane. If good KAM surfaces exist χ can change by at most an angle of π, due to their relative velocity in the angular coordinate. However two orbits within an island rotate around one another with χ increasing with the rotation about the island O-point,

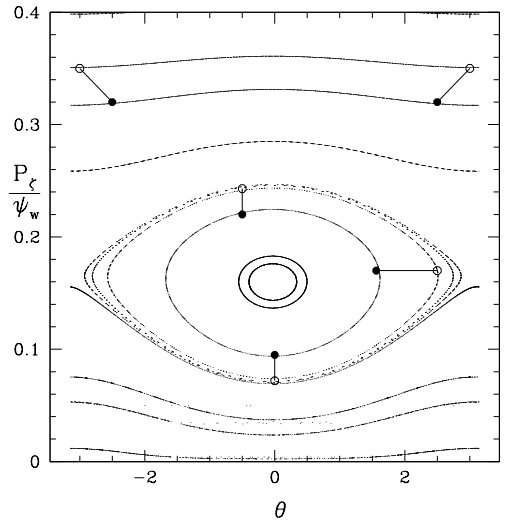

FIG. 2: The P_ζ, θ plane showing a single $m = 1$ resonance island, and vectors between nearby points on good KAM surfaces and in the island. On nearby KAM surfaces the phase vector can rotate by at most π, whereas a phase vector in an island rotates through 2π with a period given by the trapping bounce time.

also refered to as the bounce frequency of a particle trapped in the wave, which increases with the size of the island. The rate of change of χ is a function of distance from the island O-point, dropping to zero at the separatrix. This is illustrated in Fig. 2, showing vectors between nearby points in the P_ζ, θ plane on good KAM surfaces and in a resonance. Thus we determine the nonexistence of good KAM surfaces by examining nearby pairs of orbits, looking for phase vector rotation χ exceeding π.

An example of such a determination is given in Figure 3. A simple circular equilibrium was used, with the q profile equal to 1 on axis and to 5 at the plasma edge. Shown is a Poincaré plot of the field, produced by three zero frequency tearing modes with $m/n = 1/1$, $m/n = 3/2$ and $m/n = 2/1$. First order Fibonacci resonances ($\sim \alpha^2$) are thus produced at 4/3 and 5/3 and the next order ($\sim \alpha^3$) gives islands at 5/4, 7/5, 8/5, and 7/4. The Poincaré plot shows the three lowest order resonances and also the 5/3 resonance at $P_\zeta = -0.5$. Barely visible is the 7/5 resonance at $P_\zeta = -0.39$ caused by coupling of 4/3 and 3/2 and other high order resonances are not visible with this resolution.

In addition we show the result of the phase vector rotation criterion. Superimposed on a Poincaré plot are points obtained by launching pairs of particles distributed in P_ζ, θ,

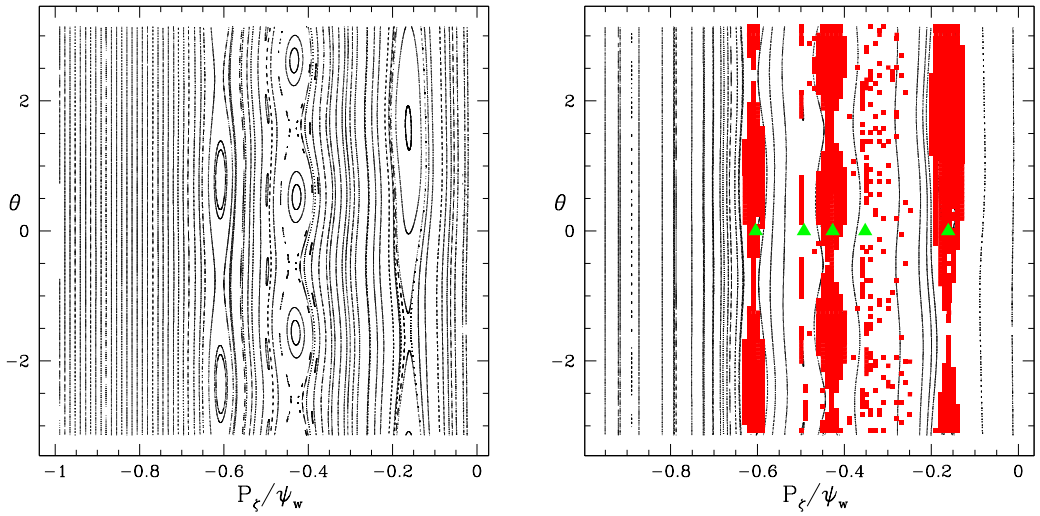

FIG. 3: Kinetic Poincaré for 2/1, 3/2 and 1/1 tearing modes with $\omega = 0$, and amplitudes $\alpha = 10^{-5}R$, and rotation indicator. Resonant surfaces from Eq. 8 are also shown with large triangles for surfaces 2/1, 5/3, 3/2, 4/3, and 1/1, listed in order from the left in the plot.

and recording only those initial values participating in phase vector rotation. The major resonances at 2/1, 3/2 and 1/1 as well as the higher order resonances at 5/3 and 4/3 are clearly seen. The 4/3 is more visible in the phase vector rotation plot than in the Poincaré plot. Also shown with large triangles are the locations of the resonances for 2/1, 5/3, 3/2, 4/3, and 1/1 from Eq. 8.

For this plot the particle energy was taken very small and all particles have pitch equal to one, so that the orbits simply follow field lines. Since for very small islands the phase vector rotation is very slow, the particles must be followed for a longer time to detect smaller islands, and the length of the simulation is determined by the desired resolution. In addition, islands smaller than the separation between the pairs of orbits are of course not detectable. The separation cannot be chosen too small or it will result in false positive island detection due to numerical error. Thus there are three parameters to adjust for an optimization of this procedure; the initial orbit pair separation, the number of toroidal transits followed, and the critical value of rotation to indicate KAM destruction. For the present work we have chosen a separation of 2×10^{-4} times the minor radius, a run time of 500 toroidal transits, and a critical value of rotation of $|d\chi| = 4$. Optimal values of these parameters depend on the spectrum of perturbations studied, and must be adjusted so that the regions of good and

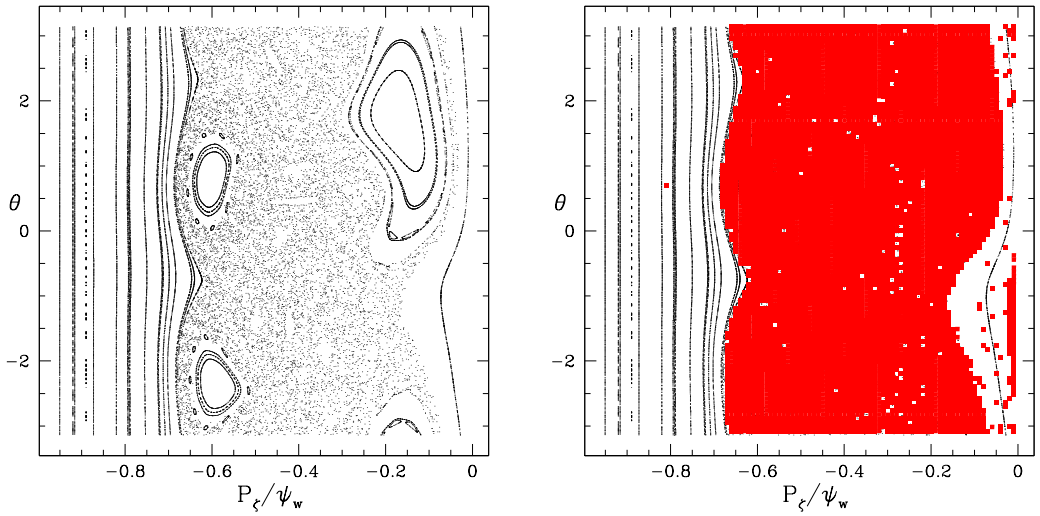

FIG. 4: Kinetic Poincaré plots for a global perturbation with 1/1, 3/2 and 2/1 tearing modes with $\omega = 0$, and phase vector rotation indicator, with larger amplitude, so islands overlap. Rotation is seen also to reliably indicate the stochastic region.

broken KAM surfaces agree with kinetic Poincaré plots showing the phase space structure to within the desired resolution.

If the mode amplitudes are increased so that a stochastic region is produced, even more KAM surfaces are destroyed. In Fig. 4 is shown a plot with amplitudes of the 1/1, 3/2 and 2/1 modes of Fig. 3 multiplied by ten, and thus island size by about a factor of three. In this case the islands overlap, and the Chirikov criterion is well satisfied. We see that the criterion of looking for phase vector rotation also reproduces the stochastic region, that is the lack of rotation is a necessary condition for the existence of a good KAM surface. Note that the region in P_ζ is not simple, since it is dependent on the mode phase, so that for given P_ζ the region is θ dependent. We wish to define domains in the space of P_ζ, E using this method, close to the maximum extent of the island or stochastic region, so a few particle pairs are initiated in each domain with random phase with respect to the perturbations, the rotation of any pair indicating broken KAM surfaces for the domain.

III. MULTIPLE MODES

If two perturbations have the same values of ω/n a single kinetic Poincaré plot can show the interaction of the modes and any produced stochastic domains, as demonstrated in Fig.

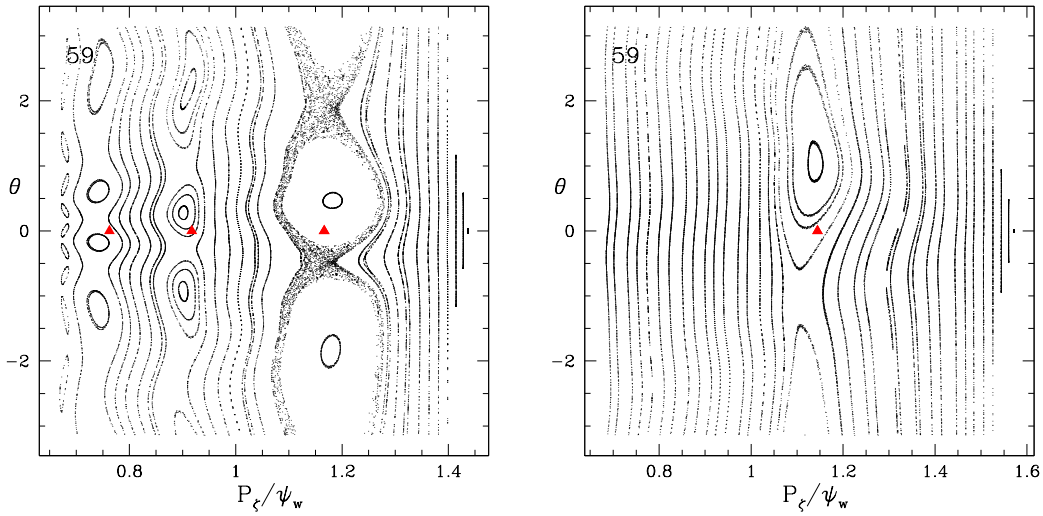

FIG. 5: Kinetic Poincaré plots for a 100 kHz global perturbation with $m/n = 3/2$, 100 kHz, and one with $m/n = 2/1$, 100 kHz. Both modes produce a large island chain at $P_\zeta \simeq 1.15$. Resonance locations from Eq. 8 are shown for $m'/n = 4/2$, $3/2$, $2/2$ in the left plot and $m'/n = 1/1$ in the right.

4. With modes of different values of ω/n it is not so easy to assess the effect of their mutual presence. Shown in Fig. 5 are the effects of two large amplitude modes, on the left the kinetic Poincaré plot of a $m/n = 3/2$ perturbation and on the right the kinetic Poincaré plot of a $m/n = 2/1$ perturbation, each with frequency of 100 kHz. The particle distributions for the two Poincaré plots have a fixed value of μB_0 of 20 keV with B_0 the on-axis value of the field and E = 59 keV at the plasma edge at the outboard midplane. A simple circular equilibrium was used with $0.8 < q < 4$ and $B_0 = 20kG$. Resonance locations from Eq. 8 are shown for $m'/n = 4/2$, $3/2$, $2/2$ in the left plot and $m'/n = 1/1$ in the right. For all these resonances $l = 1$. We see that Eq. 8 is reasonably accurate in predicting resonance location.

If both modes are present the resulting effect cannot be shown in a single Poincaré plot. The modes are chosen large enough so that the large islands near $P_\zeta = 1.15$ clearly overlap. If these perturbations had the same values of ω/n the Chirikov overlap criterion would indicate a large stochastic domain similar to that shown in Fig. 4.

In Fig. 6 are shown the modifications of the two particle distributions in the presence of both modes. On the left is shown the full long time evolution of the distribution initiated with $dE/dP_\zeta = \omega$. This initial distribution is that necessary for producing a Poincaré plot

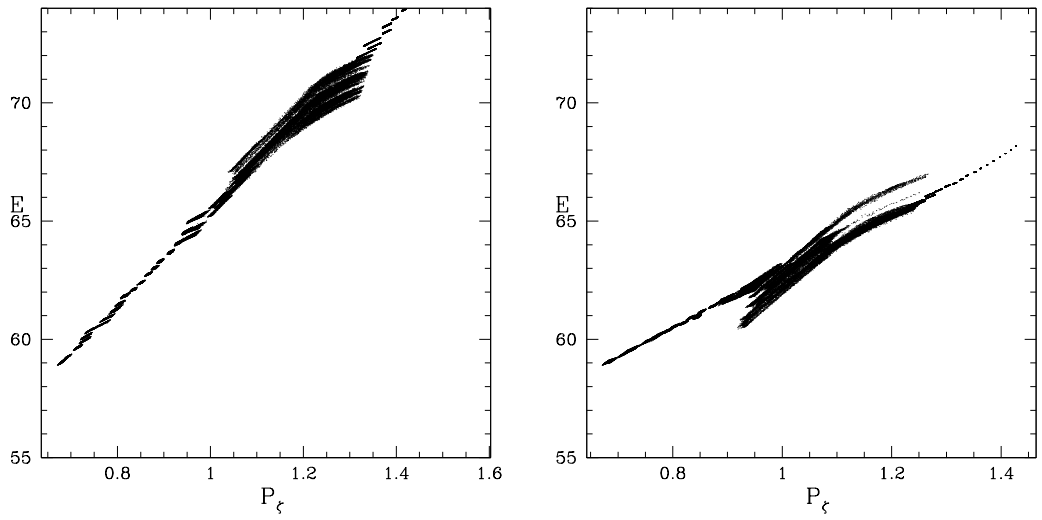

FIG. 6: Particle distributions, showing particle paths with $m/n = 3/2$, 100 kHz and $m/n = 2/1$, 100 kHz modes together. In the plot on the left the initial distribution is along a line with $dE/dP_\zeta = \omega$, and on the right the initial distribution is along a line with $dE/dP_\zeta = \omega/2$.

corresponding to the $n = 1$ mode with $\omega P_\zeta - nE = c$. The $n = 1$ mode by itself can move particles only along the line of the initial deposition. Seen near $P_\zeta = 1.2$ are particles that have been moved along the line $dE/dP_\zeta = \omega/2$, the effect of the $n = 2$ mode, due to the large island produced by this perturbation at that location. Smaller effects are also seen at $P_\zeta = 0.7$ and at $P_\zeta = 0.81$. The resulting motion is diffusion produced by combined motion along the two lines $dE/dP_\zeta = \omega$ and $dE/dP_\zeta = \omega/2$. Note the presence of significant correlations and structure, not simple stochastic motion in the two possible directions.

Similarly, on the right is the modification of the initial distribution with $dE/dP_\zeta = \omega/2$, necessary for producing a Poincaré plot corresponding to the $n = 2$ mode. This distribution can be moved only along this line by the $n = 2$ mode, but it is seen that near $P_\zeta = 1.0$ particles are also moved along $dE/dP_\zeta = \omega$, the effect of the $n = 1$ mode. Once again one notes the presence of significant correlations and structure, not stochastic motion in the two possible directions.

In Fig. 7 is shown the evolution of $< dE^2 >$, $< dP_\zeta^2 >$, and $< dE dP_\zeta >$, for those particles of Fig. 6 along the line $dE/dP_\zeta = \omega/2$ with the initial energy between 63 and 64 keV, where the brackets indicate an average over the full particle distribution. The values of dP have been multiplied by 10 to keep all data on the same plot. There is seen to be an

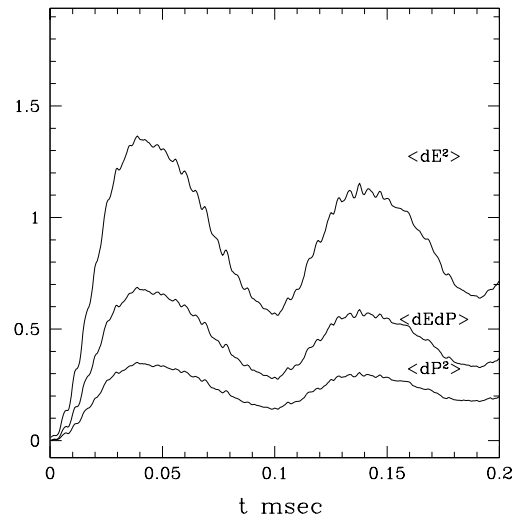

FIG. 7: Evolution of E and P_ζ, with $m/n = 3/2$, 100 kHz and $m/n = 2/1$, 100 kHz modes together.

initial ballistic period with dE and $dP_\zeta \sim t$ followed by a fairly linear evolution of all three variables, during which time one can estimate diffusion values. The value of $< dEdP_\zeta >$ is intermediate between $< dE^2 >$ and $< dP_\zeta^2 >$ indicating strong correlation, because motion can only occur along the two lines $\omega/2$ and ω. Finally the variables reach the boundary of the transport domain and settle to steady state values after bouncing for some time in the transport domain, indicating that there is phase memory during the first few transits of the domain. If this same simulation is repeated with only one mode present the excursions are orders of magnitude smaller and do not resemble diffusive motion. Thus we conclude that two such modes indeed interact, producing a limited domain in which the particle motion is highly diffusive, although still with strong correlations. The interaction of the two modes is motion along the two different lines in the P_ζ, E plane, each step in one direction by one mode moving to a different part of the island produced by the other mode, thus allowing the distribution to explore the full range of both islands, rather than simply experiencing phase mixing and flattening in a single island. In realistic cases there are not only two such modes, but an entire spectrum, each with its lines in the P_ζ, E plane.

To confirm the nature of the motion, perform a quasilinear approximation for the diffusion in energy. We have a perturbation of the form $\delta\vec{B} = \nabla \times \alpha\vec{B}$ with $\alpha = \sum_{m,n} \alpha_{m,n}(\psi_p) sin(n\zeta - m\theta - \omega_n t)$ where α has the units of length. The energy change

is given by

$$dE/dt = -\rho_{\|} B^2 \partial_t \alpha + \partial_t \Phi. \tag{11}$$

The units of length are in terms of the major radius R and time is in terms of the on axis cyclotron frequency ω_0, so the energy is in terms of $M\omega_0^2 R^2$ with M the particle mass. The potential is given in Boozer coordinates by $(gq + I)\omega\alpha_{m,n} = (nq - m)\Phi_{m,n}$, giving

$$dE = A_{mn} cos(n\zeta - m\theta - \omega_n t)dt \tag{12}$$

with $A_{mn} = [\rho_{\|} B^2 + (gq + I)\omega_n/(nq - m)]\omega_n \alpha_{mn}$. The quasilinear approximation gives

$$< E^2 >= \sum_{mn} \frac{A_{mn}^2}{4\pi\omega_n} t. \tag{13}$$

Make a simple estimate. Note that the particle energies are above 60 keV, much larger than μB_0, so the particles are deeply passing and $\rho_{\|} B \sim v$, and the contribution of the potential is of the order or smaller than that due to δB, giving $A_{mn}^2 \sim 2(E/M)B^2\omega_n^2\alpha_{mn}^2$, and for the diffusion

$$< E^2 >= \sum_{mn} (E/M)B^2\alpha_{mn}^2(\omega_n/2\pi)t. \tag{14}$$

Reinserting units using $\alpha_{mn} = 2 \times 10^{-5} R$, $B = M\omega_0$ and using $M\omega_0^2 R^2 = Mc^2\omega_0^2 R^2/c^2$, with a plasma of deuterium so $Mc^2 = 1862 Mev$, $\omega_0 = 9.3 \times 10^7/sec$, $R = 100cm$, $E = 60keV$, $(\omega_n/2\pi) = f_n = 100kHz$ we find

$$\frac{< E^2 >}{t} = \sum_{mn} EMc^2(\omega_0^2 R^2/c^2)(\alpha_{mn}^2/R^2) f_n \tag{15}$$

or $< E^2 > \sim 40keV^2 t(msec)$ in reasonable agreement with Fig. 7. Thus we conclude that overlap of resonance due to modes of different frequencies results in significant stochastization of particle orbits, as the naive application of the Chirikov overlap criterion would indicate. For these incommensurate modes the process is diffusion in a higher dimension and can be treated using what is called the stochastic pump model[14], by successively finding the motion due to each perturbation.

IV. CONFIRMATION OF THE PHASE VECTOR ROTATION CRITERION

Now we carry out a test of this procedure using the DIII-D reversed shear equilibrium for shot 122117 shown in Fig. 8, along with the q profile, considered in [2, 3]. We consider one

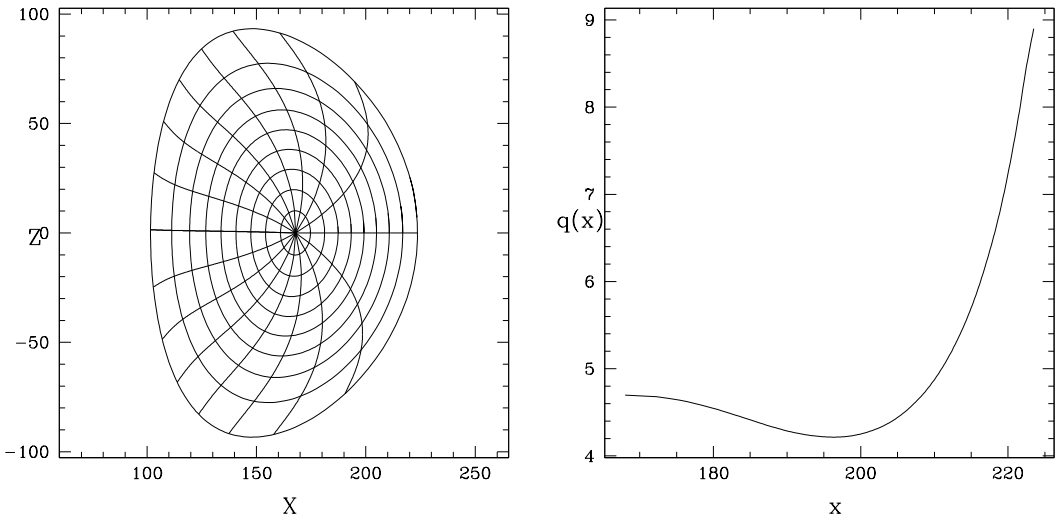

FIG. 8: DIII-D reversed shear equilibrium and q profile for shot 122117.

of the eleven TAE and RSAE modes present in this discharge. The phase vector rotation determination was performed using 100 domains in energy, from 20 to 60 keV and also 100 domains in canonical momentum. The initial pair separation was $\Delta\psi_p = 2 \times 10^{-4}\psi_w$, where ψ_w is the magnitude of the poloidal flux at the last flux surface. Two particle pairs were deposited in each domain, initiated at $\theta = 0$ but with random ζ so that each pair has a different phase relation with the mode. The run time was chosen to be 500 toroidal transits. Any orbit pair exhibiting phase vector rotation greater than $|\chi| = 4$ causes that domain to be labeled non-KAM. Only positive pitch was used, so that this analysis is restricted to trapped and co-passing particles, neglecting the counter passing population.

The poloidal harmonics of the TAE mode are shown in Fig. 9. The mode had a frequency of 81 kHz with $n = 3$. The mode is located near the plasma center in the region of reversed shear. We examine the resonances due to the mode spectrum using both the phase vector rotation and kinetic Poincaré plots, to determine the validity of the use of the rotation to find broken KAM surface domains. Shown in Fig. 10 is the E, P_ζ plane showing the result of the phase vector rotation determination for a distribution with $\mu B_0 = 14keV$ and three kinetic Poincaré plots showing the nature of the resonances along lines with $\omega P_\zeta - nE = constant$, with energies at the left (end point of the Poincaré plot) of 44, 35 and 25 keV. The domains in the E, P_ζ plane are shaded where phase vector rotation indicated broken KAM surfaces.

The first Poincaré figure, showing the plot for the line starting at 44 keV, shows a small

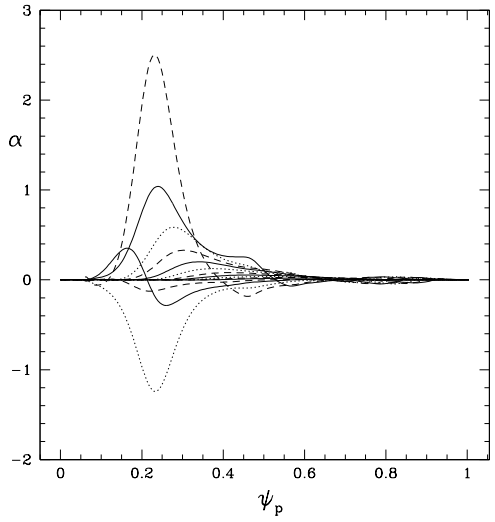

FIG. 9: Poloidal harmonics ($\times 10^{-6}$) of an 81 kHz $n = 1$ TAE mode with $10 \leq m \leq 23$, observed in DIII-D in shot 122117.

$m'/n = 12/3$ resonance at P_ζ = -0.16, a small $m'/n = 11/3$ resonance at P_ζ = -0.02, a small $m'/n = 10/3$ resonance at $P_\zeta = 0.26$, and a large $m'/n = 10/3$ resonance at $P_\zeta = 0.47$. All of these resonances are clearly visible in the P_ζ, E plane, and exist continuously for a large range of energies.

The second plot, for the line starting at 35 keV, shows the same small ten island resonance seen in the first plot, now at P_ζ = -0.02, and the same large ten island resonance now at $P_\zeta = 0.45$.

The third plot, for the line starting at 25 keV, shows a large nine island resonance at $P_\zeta = 0.21$. Note that the large resonance near the plasma center has $m' = 10$ above 35 keV, then there is a break with no resonance near 30 keV, and it resumes as a $m' = 9$ resonance between 25 and 30 keV. Again there is a break, and the resonance seen in the P_ζ, E plane at 22 keV has $m' = 8$.

Now we examine a part of the distribution including trapped particles. Shown in Fig. 11 is the E, P_ζ plane showing the result of the phase vector rotation determination for a distribution with $\mu B_0 = 30keV$ and three kinetic Poincaré plots showing the nature of the resonances along lines with $\omega P_\zeta - nE = constant$, with energies at the left (end point of the Poincaré plot) of 36, 30 and 26 keV. The domains in the E, P_ζ plane are shaded where phase vector rotation indicated broken KAM surfaces. In this case the distribution contains many trapped particles.

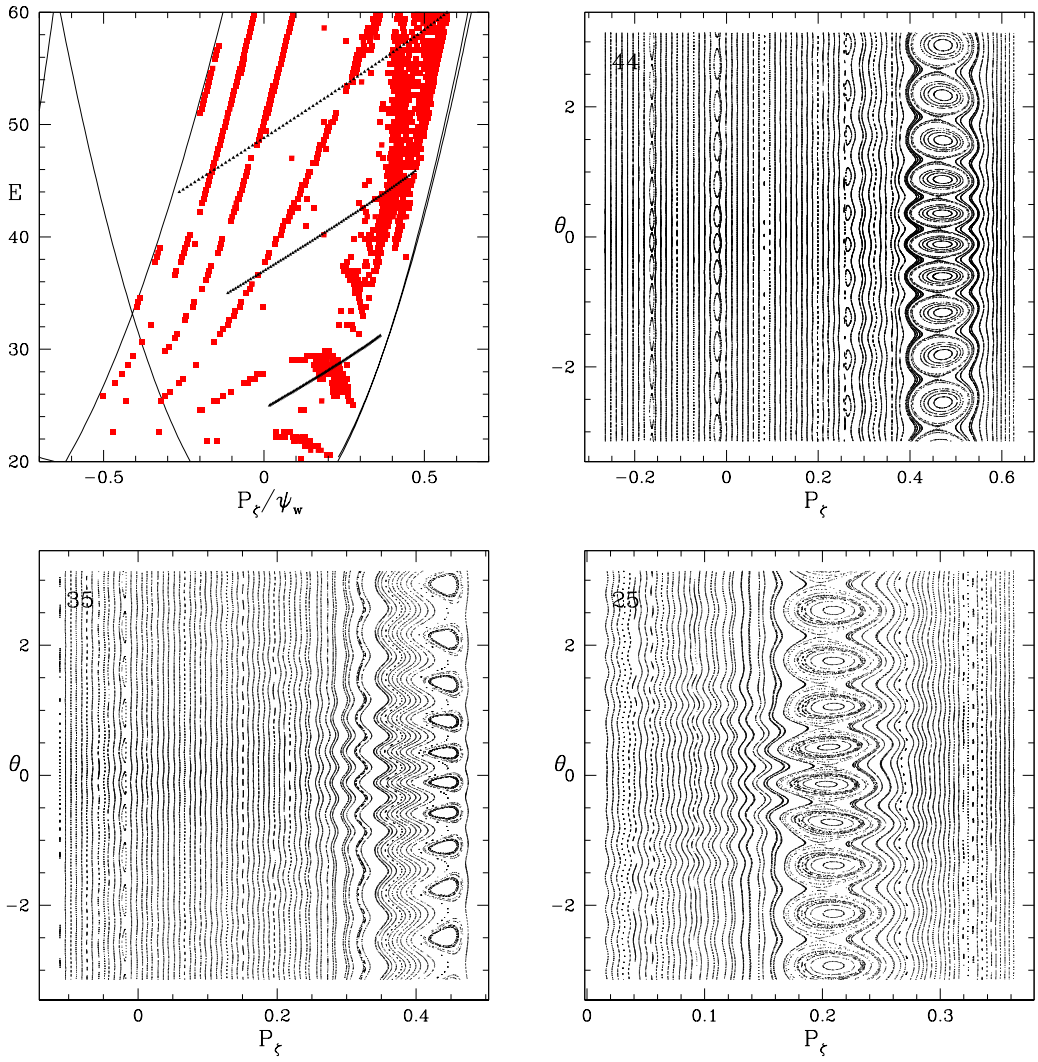

FIG. 10: Plane of P_ζ, E with $\mu B_0 = 14keV$, for the 81 kHz $n = 1$ TAE mode with $10 \leq m \leq 23$ observed in DIII-D in shot 122117, showing paths for kinetic Poincaré plots for the three lines originating at the left at 44, 35 and 25 keV. Also shown are the three Poincaré plots associated with these lines.

The first Poincaré figure, showing the plot for the line starting at 36 keV, shows a dense series of resonances existing in the trapped domain. The size and proximity of these resonances are such that they are not resolved in the E, P_ζ plane with the domain size used.

The second plot, for the line starting at 35 keV, shows a dense series of resonances existing in the trapped domain, again partly not resolved in the E, P_ζ plane. There is a large $m' = 8$ resonance in the passing domain at 36 keV, probably the same resonance also visible in Fig. 10 at 22 keV.

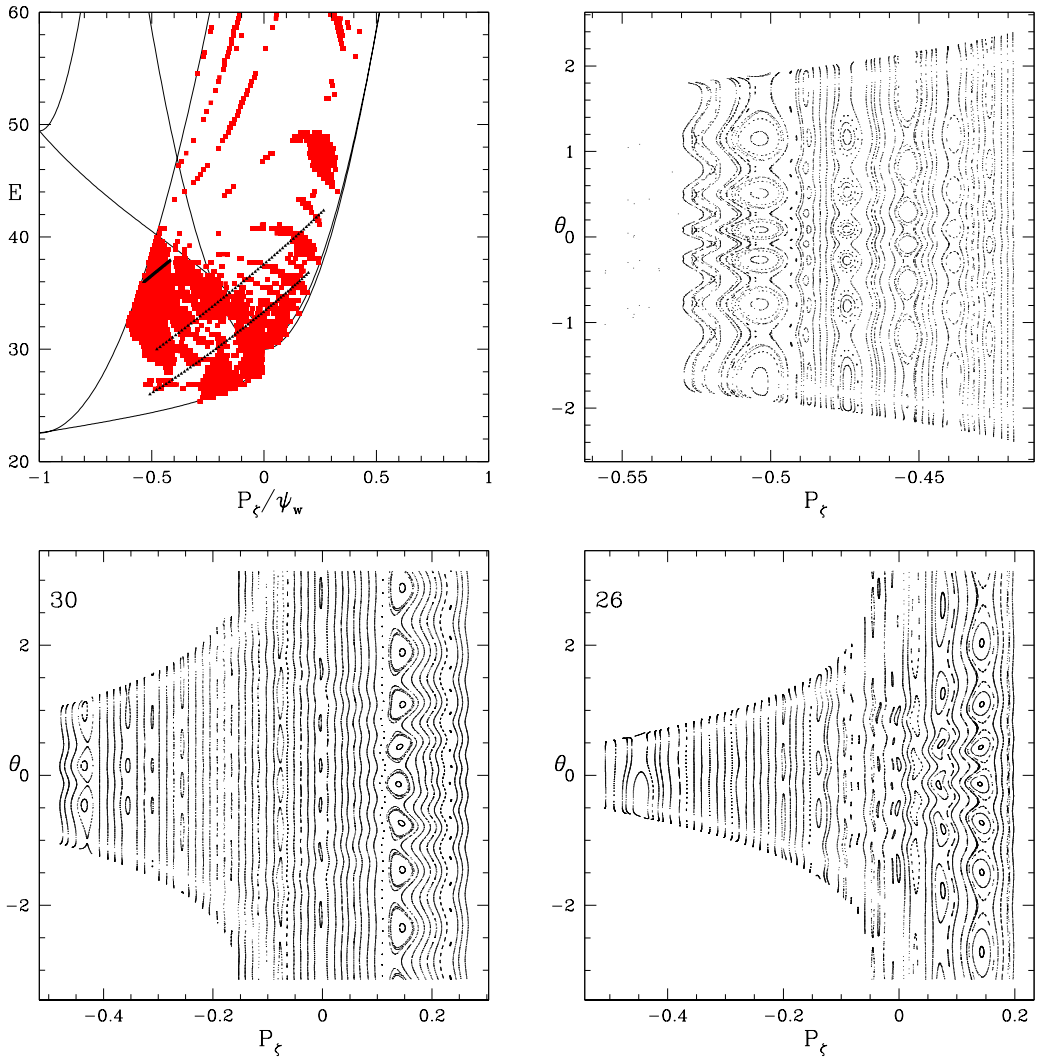

FIG. 11: Plane of P_ζ, E with $\mu B_0 = 30KeV$, for the 81 kHz $n = 1$ TAE mode with $10 \leq m \leq 23$ showing three paths for kinetic Poincaré plots originating at the left at 36, 30 and 26 keV, and the three Poincaré plots produced along these lines.

The third plot, for the line starting at 26 keV, shows a $m' = 1$ resonance at P_ζ = -0.45 and many small resonances near the trapped passing boundary, along with larger $m' = 5$, $m' = 6$ and $m' = 7$ resonances in the passing domain.

Many of the resonances in the trapped particle region are too small and too close together for resolution using the phase vector rotation. On the other hand the actual particle distribution is sparse in this region, so it is not clear that failure to completely resolve these resonances presents a problem for calculating the final relaxed state of the distribution under the effect of these modes. A complete analysis of this problem must await a future

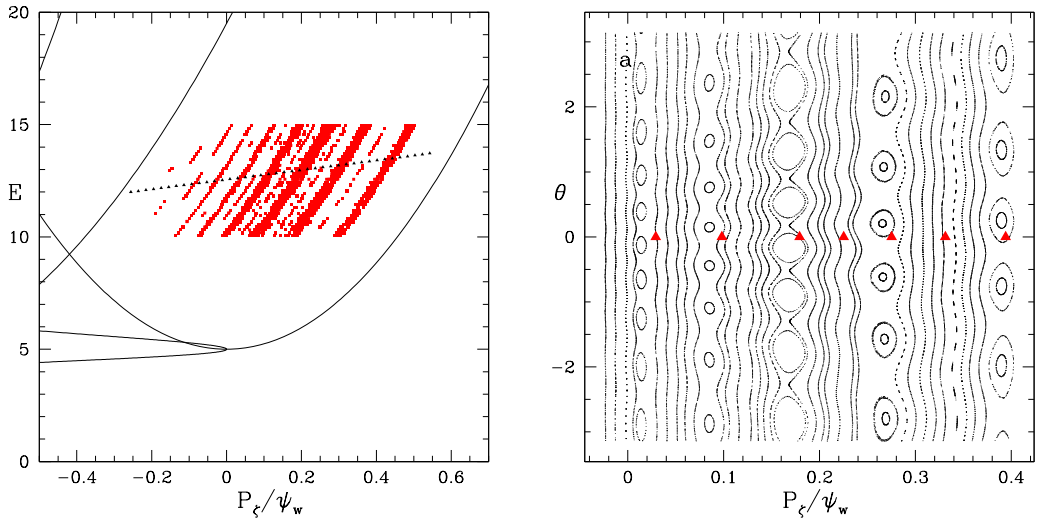

FIG. 12: Plane of P_ζ, E with $\mu B_0 = 5KeV$, for a 10 kHz local mode with $m/n = 6/5$ and amplitude $\alpha = 5 \times 10^{-6} R$ and a kinetic Poincaré plot made along the line originating at the wall at 12 keV. Resonance locations from Eq. 8 are shown for m'/n = 9/5, 8/5, 7/5, 6/5, and 5/5, and also, at points were no island is visible in this plot, for $m'/nl = 13/10$, and $m'/nl = 11/10$.

publication.

V. AVALANCHE

Now we wish to investigate the approach to avalanche conditions due to several resonance island chains. For this we again use a simple circular equilibrium with $0.8 < q < 4$. In Fig. 12 are shown the results of the phase vector rotation determination for a single broad 10 kHz mode with $m/n = 6/5$, with amplitude of $\alpha = 5 \times 10^{-6} R$ and kinetic Poincaré plots showing the nature of the resonances. In Fig. 12 resonance locations from Eq. 8 are shown for m'/n = 9/5, 8/5, 7/5, 6/5, and 5/5. Also appearing between 7/5 and 6/5 is a second order Fibonacci resonance point for $m'/nl = 13/10$, and between 6/5 and 5/5 one for $m'/nl = 11/10$, but no islands visible at these surfaces in this plot. Island widths are comparable for $m' = m, m \pm 1$ and somewhat smaller for $m' = m + 2, m + 3$. The surfaces for resonances with $m' = m - 2, m - 3$ are outside the plasma. In the plane of P_ζ, E the major resonances are clearly visible as well as the first order Fibonacci sequence, appearing as thinner partly broken lines in between the major broader resonances. The phase vector rotation indicates that islands exist at $m'/nl = 13/10$, and at $m'/nl = 11/10$ but they are

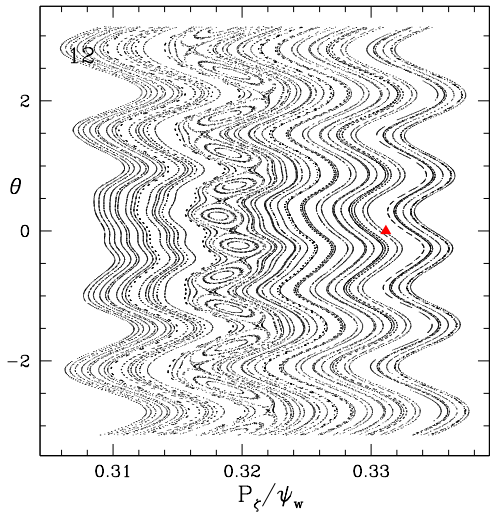

FIG. 13: Blow up of the Poincaré plot of Fig. 12 showing the $m'/nl = 11/10$ visible in the plane of P_ζ, E in Fig. 12. Also shown is the resonance point from Eq. 8.

not visible in this Poincaré plot.

In Fig. 13 is a blow up of the region around $P_\zeta = 0.32$, showing that in fact the $m'/nl = 11/10$ resonance visible in the plane of P_ζ, E is present. The phase vector rotation criterion appears to be reasonably sensitive. The island width is about $0.02\psi_w$, well above the particle pair separation of $2 \times 10^{-4}\psi_w$. This corresponds to an island of about one centimeter width in DIII-D. Note however that the resonance location as given by Eq. 8 is incorrect by a few times the width of the island.

In Fig. 14, with the mode amplitude ten times larger, a continuous stochastic domain has appeared between $P_\zeta = 0.05$ and $P_\zeta = 0.42$, containing remnant islands from the major resonances. On the left are still visible a $m'/n = 9/5$ and a $m'/n = 10/5$ island chain, also visible in Fig. 12 in the P_ζ, E plane. Note that good KAM surfaces exist both near the plasma edge and near the axis, so this mode should produce only local profile flattening, but no particle loss.

For the most part the phase vector rotation appears to give a reasonable description of the non-KAM domains. It has the advantage over methods that simply determine resonance location through integrals such as Eq. 8, see also[15, 16] that the resonance is shown only if the mode is sufficiently large at the requisite surface, and in addition the full width of the resonance is displayed, not only the location. Also there can be no innacuracy regarding

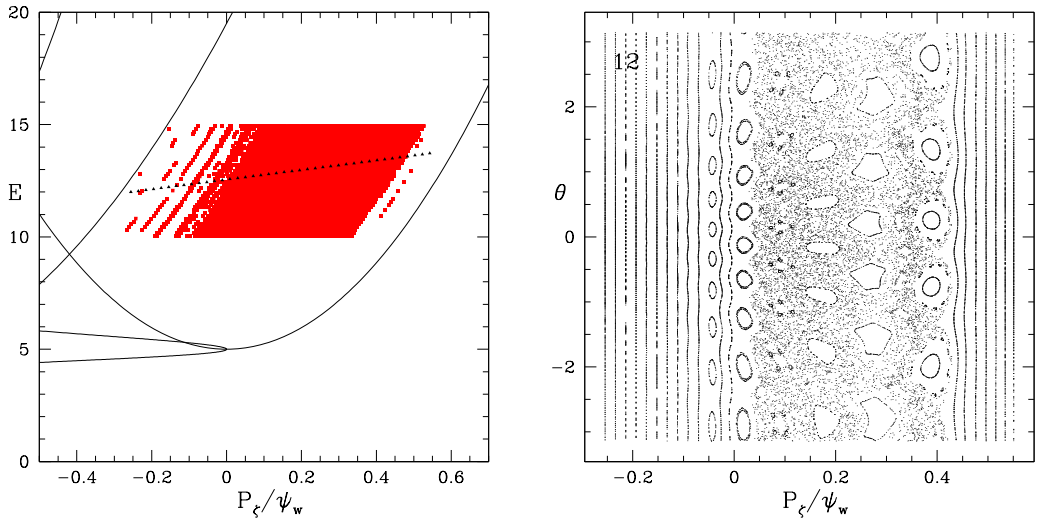

FIG. 14: Plane of P_ζ, E with $\mu B_0 = 5KeV$, for a 10 kHz local mode with $m/n = 6/5$ and a kinetic Poincaré plot for amplitude 5×10^{-5} made along the line originating at the wall at 12 keV.

the location. It thus makes evident which perturbations and nonlinear produced islands of the Fibonacci sequence should be taken into consideration. Besides this, as is evident from examples shown, resonance location is only approximate. Primary resonances are reasonably well given, but higher order resonances are often displaced significantly from the location given by Eq. 8.

If necessary, resolution can be improved significantly at some computing cost, but phase vector rotation appears to be able to detect very small island chains. In fact with the parameters used here it may be more sensitive than necessary. If only large islands are responsible for profile modification the parameters of the search can be relaxed, leading to less computation. It is not clear that the failure to observe very small domains of good KAM surfaces with the phase vector rotation is a serious problem. In any real system there are also small particle scattering processes, capable of moving particles across narrow barriers. The method should also form an important check of the first step in constructing quasilinear diffusion models of transport in such systems, which must be the determination of the location and extent of resonances.

VI. ANNEALING

We wish to use the determination of domains in the P_ζ, E plane with destroyed KAM surfaces to find the final state of a given particle distribution under the action of the mode spectrum. We are interested in collisionless effects, but we point out that pitch angle scattering, since it conserves energy, results in simple diffusion in P_ζ and μ, and can be included. Similarly it is simple to include the effect of energy loss through slowing down on electrons.

Construct a numerical method of producing the final state of a given particle distribution under the action of a given spectrum of modes. In the final state the density should be constant for a particular mode with frequency ω and toroidal mode number n, in all island and stochastic domains along lines given by $\omega P_\zeta - nE = constant$, since this combination is conserved and annealing can happen only along this line. However, as seen above, repeated annealing for multiple modes, with different values of ω/n, produces diffusive motion in the combined non-KAM domains of the modes involved. Thus the necessary algorithm must be an iterative annealing process, one mode at a time, but repeated so as to capture the effect of the combination of modes present.

Examine a high energy particle distribution as predicted by a neutral beam deposition calculation or an alpha particle birth profile calculation, and make a number of domains in the magnetic moment μ sufficient to give a good representation of the distribution. For each μ, divide the space of confined particles in the P_ζ, E plane into small domains, with size determined by the desired resolution of small islands. Then find the domains of broken KAM surfaces for that part of the plane which is occupied by the distribution by following pairs of orbits and looking for phase vector rotation, noting whether each domain is stochastic or consists of good KAM surfaces. This is the only computationally demanding part of the calculation, depending on the desired resolution for island size. Reintroduce the original distribution and distribute it into the μ, P_ζ, E domains. At this point, to improve accuracy of the annealing process the number of particles can be multiplied by a factor sufficient to make the number of particles in each domain large. Then carry out an equilibration of densities in stochastic domains which are in contact along lines $\omega P_\zeta - nE = c$ for each mode, iterating this process until a final state is achieved.

To carry this out, note that the differential volume is given by $dV = J(\psi_p, \theta) d\theta d\psi_p$, where in Boozer coordinates $JB^2 = gq + I$. Thus the domain at μ, P_ζ, E with range dP_ζ

has volume

$$dV = dP_\zeta \int d\theta \left(\frac{d\psi_p}{dP_\zeta}\right)_{E,\mu} J(\psi_p, \theta), \tag{16}$$

the integration being over the particle orbit. Using $P_\zeta = g\rho_\parallel - \psi_p$ and $E = \rho_\parallel B^2/2 + \mu B$ we find

$$dV = dP_\zeta \int d\theta \frac{(gq + I)}{B^2} \frac{1}{1 + g(\rho_\parallel^2 B + \mu)\partial_{\psi_p} B/\rho_\parallel B^2 - g'\rho_\parallel} \tag{17}$$

where the integral is taken over a constant μ, P_ζ, E surface and $g' = \partial_{\psi_p} g$. Thus in neighboring stochastic domains along the lines with $\omega P_\zeta - nE = c$ with initial particle numbers n_1, n_2 and $n_1 + n_2 = N$, particle conservation gives $n_1' + n_2' = N$ and equal densities gives $n_1'/dV_1 = n_2'/dV_2$ so the new particle numbers are

$$n_1' = \frac{N dV_1}{dV_1 + dV_2}, \qquad n_2' = \frac{N dV_2}{dV_1 + dV_2}. \tag{18}$$

In addition to replacing the densities in adjacient stochastic domains with the modified values for the two domains, stochastic domains in contact with the outer wall are emptied of particles, they being counted as lost. In the present case there are no losses because of the good KAM surfaces near the outer edge. This process must be repeated several times using the stochastic domain template for each mode. After the annealing the particle distribution can be reconstructed. Given μ, P_ζ, E the orbit is completely determined, but not the particle location on the orbit. The distribution can be reconstructed using a uniform distribution in θ. Since n_1', n_2' from Eq. 18 are not integer, reconstructing the distribution involves rounding to the nearest integer, hence the reason for making n_1, n_2 large.

To test this procedure a simple circular equilibrium with $q = 0.8$ on axis and $q = 4$ at the last closed flux surface was used, with a simple distribution with a single value of $\mu B_0 = 5KeV$ and with energy ranging from 10 to 15 keV, but with a steep density profile. The single mode of Fig. 14 was used, consisting of a large amplitude $m/n = 6/5$ localized 10 kHz perturbation. Also shown is the result of the phase vector rotation indicator. Twenty domains in energy were used, since the range of energy of the distribution was chosen to be small, and 200 domains in canonical momentum P_ζ to provide sufficient resolution. The orbit pairs were separated by $\Delta\psi_p = 2 \times 10^{-4}\psi_w$, with ψ_w the value of poloidal flux at the plasma edge. In the P_ζ, E plot a broad stochastic band is seen, as well as three narrow partly broken bands to the left of it. Note that the location of resonances in θ is at constant

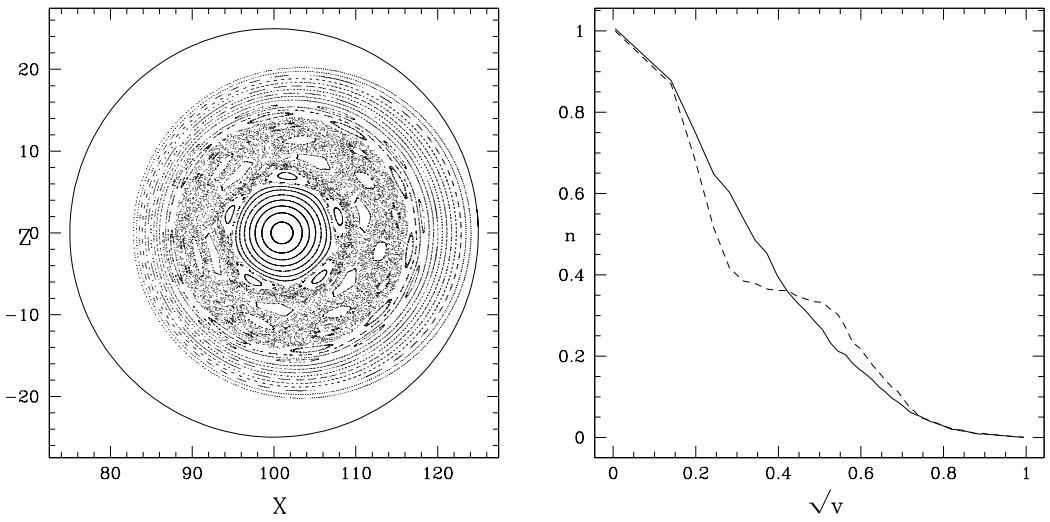

FIG. 15: The kinetic Poincaré plot of Fig. 14, shown in the X, Z plane, showing the extent of the stochastic domain, with $\mu B_0 = 5KeV$, for a local 10 kHz mode with $m/n = 6/5$, and the result of annealing. Shown is the initial distribution and that obtained using the annealing process, plotted versus the square root of the volume, approximately equal to the minor radius.

P_ζ, but not on a flux surface. The good KAM surfaces shown in the plot of the poloidal cross section in Fig. 15 do not coincide with flux surfaces, they are shifted outboard. The resonance location in the poloidal plane depends on poloidal angle, mode frequency and particle energy. The magnitude and location of the perturbation was chosen so that there are bands of good KAM surfaces both in the plasma center and near the outer edge. Thus the expected result is local flattening at the location of the stochastic domain with no induced loss.

The annealing process is carrried out repeatedly in the stochastic domains, equalizing densities along the lines $\omega P_\zeta - nE = constant$ until the particle distribution has stabilized, this process taking a very small amount of computing time. The second plot of Fig. 15 shows the initial and modified profiles of the density, obtained by binning particles using equal size bins in the volume inscribed by a given flux surface, plotted versus the square root of the volume, approximately the minor radius, showing the canonical near flattening of the distribution in the stochastic domain. The flattening is not perfect because the boundaries of the stochastic domain do not coincide with flux surfaces.

VII. CONCLUSION

In conclusion, we describe a new method for the determination of domains of broken KAM surfaces in the space of P_ζ, E, μ describing confined particles in a toroidal confinement device due to the presence of a spectrum of MHD modes. This method should be useful for the application of quasilinear diffusion calculations, the first step of which must be the determination of the location and extent of the resonances. In addition we have applied the method to the determination of the final state of a distribution in the presence of given spectrum of modes through a process of local flattening of the distribution in domains of broken KAM surfaces. The method takes significantly less time than a full simulation of the time evolution of the distribution using a guiding center code and is more instructive in that the plot of the P_ζ, E plane reveals the important resonances and their extent. In this paper we only demonstrate the use of the method. In future publications we will describe the application of the method to previously studied and well documented cases of toroidal Alfvén modes in the DIII-D tokamak[2, 3]. In particular it is necessary to make a study of the resolution necessary in the P_ζ, E plane in order to correctly predict the final distribution.

This analysis only approaches part of the problem of the modification of a distribution by MHD modes. A complete theory must include the prediction of mode spectrum including amplitudes. However note that if stochastic domains result then the original distribution used to predict the mode spectrum is modified by the modes, and the new distribution in turn will change the spectrum. In fact it is very likely that the DIII-D case previously studied[2, 3] consisted of a spectrum of MHD modes near stochastic threshold for distribution modification, with the mode amplitudes in equilibrium with the flattened profile.

Acknowledgement

This work was partially supported by the U.S. Department of Energy Grants DE-AC02-09CH11466, SC-6903402 and DE-FC02-04ER54698.

The author is indebted to Phil Morrison for many enjoyable chaotic conversations.

---

[1] W. W. Heidbrink, *Phys. Plasmas* **15**, 055501 (2008), and references therein.

[2] R. B. White, N. N. Gorelenkov, W. W. Heidbrink, M. A. Van Zeeland, *Phys. of Plasmas* **17** 056107 (2010)

[3] R. B. White, N. N. Gorelenkov, W. W. Heidbrink, M. A. Van Zeeland, *Plasmas Physics Controlled Fusion* **52** 045012 (2010)

[4] M. A. Van Zeeland et al, *Phys. of Plasmas* **xx** xxx (2011)

[5] E. P. Fredrickson et al, *Phys. of Plasmas* **16** 122505 (2009)

[6] H. L. Berk et al, *Nucl. Fusion* **35** 1661 (1995)

[7] J. Fitzpatrick *A Numerical Model of Wave-Induced Fast Particle Transport in a Fusion Plasma.* PhD Thesis, University of California Berkeley (1997)

[8] A. N. Kolmogorov, *Proc. Int. Congr. Mathematicians, Amsterdam, Vol 1* 315 (1957), V. I. Arnold, *Russ. Math. Surv.* 18(5):9, 1963, J. Moser, *Math. Phys. Kl. II 1,1 Kl(1):1*, 1962,

[9] R. B. White, *High Energy Particles in Tokamaks*, *Proceedings of the first ITER Summer School*, Aix en Provence, 2008.

[10] R. B. White, *The Theory of Toroidally Confined Plasmas, revised second edition*, Imperial College Press, p. 73 (2006)

[11] R. B. White, M.S. Chance, *Phys. Fluids* **27**, 2455 (1984).

[12] M. N. Rosenbluth, R.Z Sagdeev, J.B. Taylor, G M Zaslavsky *Nuclear Fusion* **6** 297 (1966)

[13] B. V. Chirikov, *Phys. Rep.* **52** 263 (1979)

[14] A. J. Lichtenberg and M. A. Lieberman, *Regular and Chaotic Dynamics, second edition*, Springer Verlag, p. 386 (1992)

[15] W. W. Heidbrink et al, *Phys. of Plasmas* **15** 055501 (2008)

[16] Y. Todo and T. Sato, *Phys. of Plasmas* **5** 1321 (1998)

The Princeton Plasma Physics Laboratory is operated
by Princeton University under contract
with the U.S. Department of Energy.

Information Services
Princeton Plasma Physics Laboratory
P.O. Box 451
Princeton, NJ 08543

Phone: 609-243-2245
Fax: 609-243-2751
e-mail: pppl_info@pppl.gov
Internet Address: http://www.pppl.gov